Scripta Materialia 204 (2021) 114142

Contents lists available at ScienceDirect

Scripta Materialia

journal homepage: www.elsevier.com/locate/scriptamat

Revealing tribo–oxidation mechanisms of the copper–WC system under high tribological loading

X. Chen [a,*], Y. Ma [b,c,*], Y. Yang [a], A. Meng [a], Z.X. Han [d], Z. Han [d], Y.H. Zhao [a,*]

[a] Nano and Heterogeneous Materials Center, School of Materials Science and Engineering, Nanjing University of Science and Technology, Nanjing 210094, China
[b] Steel Institute (IEHK), RWTH Aachen University, Intzestraße 1, Aachen 52072 Germany
[c] Max-Planck-Institut für Eisenforschung GmbH (MPIE), Max-Planck-Str. 1, Düsseldorf D-40237 Germany
[d] Shenyang National Laboratory for Materials Science, Institute of Metal Research, Chinese Academy of Sciences, 72 Wenhua Road, Shenyang 110016, China

ARTICLE INFO

Article history:
Received 24 December 2020
Revised 13 June 2021
Accepted 7 July 2021
Available online 22 July 2021

Keywords:
Tribology
Oxidation
Transmission electron microscopy (TEM)
Atom probe tomography
Copper

ABSTRACT

The near-surface structural and chemical changes were investigated for pure copper against a tungsten carbide (WC) sphere during high tribological loading. Fundamental stages are identified in the Cu-WC tribo-system: (i) high tribological stress promotes grain refinement to the ultra-fine grains regime in the very beginning; (ii) nucleation of extremely fine (~3 nm) oxygen–enriched Cu nano particles in the near-surface layer and subsequent growth of the Cu_2O oxide; (iii) formation of continuous nanostructured mixing layer with heterogeneous Cu and O distribution in the late stage. Near-surface mechanical mixing is presumably the main contribution to chemical modifications under high tribological loading. Our findings shed atomic-insights into intricate tribochemical modifications, one of the most intriguing phenomena in material-oriented tribology.

Within the domain of tribology, one intriguing phenomenon is sliding contact introduces pronounced structural and chemical modifications into the near-surface region of base materials, wherein their products "tribolayers" will substantially alter the tribological performance [1–3]. Friction and wear reductions are largely associated with nanostructured tribolayers that form on contacting metallic surfaces in the existing literature [4–8]. A plethora of investigations indicate the formation of tribolayers stems from the involvement of basic processes such as plastic deformation [9], microstructural refinement [10], chemical reactions and mechanical mixing [11,12], etc. These manifold processes are not just thermally driven, but also triggered by the shear occurring at the contacting interfaces [11], which is inherent to a tribological load.

Particularly, the chemical compositions of the tribolayers are altered by interactions with the counterbody and the environment, including the ambient atmosphere and chemical species in lubricants [13]. Surface oxides - widely observed in the topmost tribolayer - directly confirm the interactions with the environment during sliding. Note that the oxidized tribolayer (e.g. glaze layer) can prevent direct metal-on-metal contact under mild sliding with low wear rates [14], but is susceptible to cracking as they are less ductile under high tribological loading, where the applied stress is far above the yield stress of the base material [15]. During the past decades, several hypotheses have been proposed to be responsible for chemical changes through tribological loading, like mechanical mixing [11], material transfer [16], shear-driven chemical reactions [17], and thermal diffusion [18] etc. As early as in 1956, Kerridge and Lancaster [16] highlighted the imperative role of transfer in worn surfaces of the brass pins sliding against steel rings using radioactivity methods. Later on, Rigney pointed out that sliding gives rise to vorticity in the near-surface area and thus facilitates mechanical mixing in a tribological system corroborated by molecular dynamics (MD) simulations [9]. Grain induced plastic instability and grain boundary activities were also suggested to be primarily attributable to the flow instabilities (e.g. vorticity) during sliding [19]. More recently, to better understand tribo-induced chemical changes and correlate their composition with friction and wear behavior, advanced surface characterization has become an indispensable analytical tool [20,21]. For instance, a scenario was experimentally proposed through transmission electron microscope (TEM) that diffusion of oxygen brings about the nucleation of amorphous oxide and growth of Cu_2O nanocrystals in the topmost layer of copper during mild sliding against a sapphire ball [20]. However, the mechanisms for chemical modifications are by no means simple and remain largely speculative in nature, es-

* Corresponding author.
E-mail addresses: xiang.chen@njust.edu.cn (X. Chen), y.ma@mpie.de (Y. Ma), yhzhao@njust.edu.cn (Y.H. Zhao).

https://doi.org/10.1016/j.scriptamat.2021.114142
1359-6462/

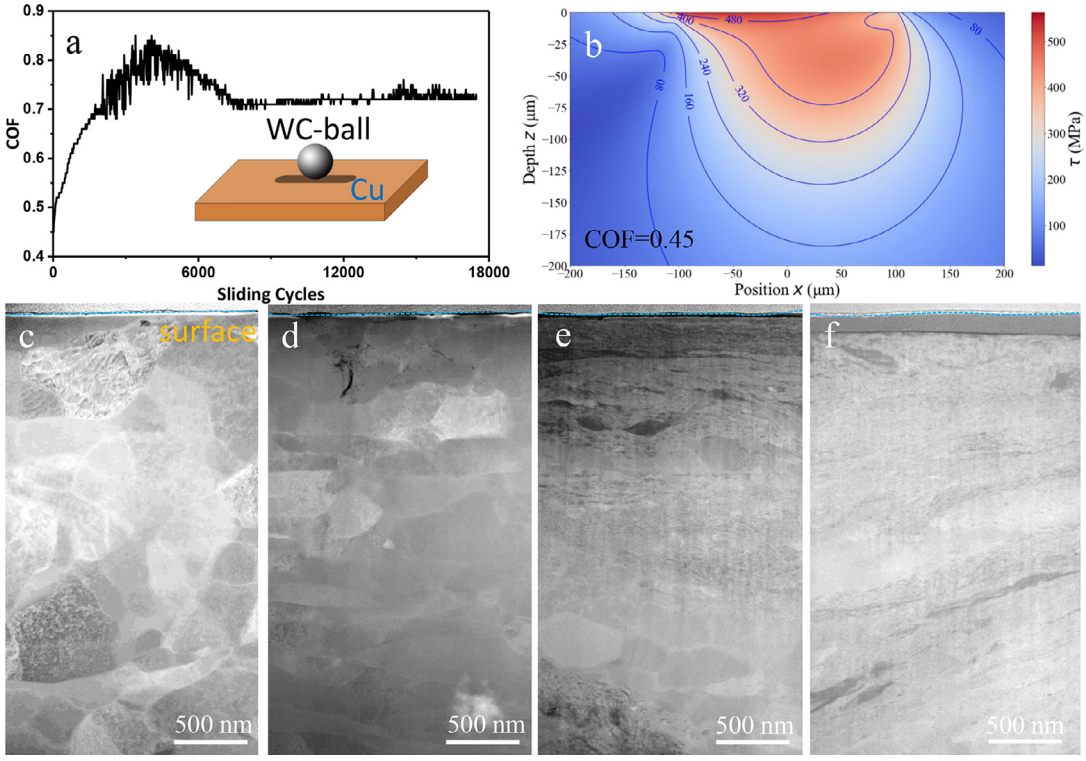

Fig. 1. (a) A typical friction curve for pure copper sliding against a WC ball under a load of 30 N and a sliding speed of 10 mm/s. (b) The τ-component of the stress field along the sliding direction for COF = 0.45. (c–f) Worn subsurface STEM images of the samples after different sliding cycles: (c) 300 cycles; (d) 3000 cycles; (e) 6000 cycles; (f) 18000 cycles. The sliding surface is outlined by the light blue dashed lines.

pecially pertaining to the very early stages under high tribological loading.

In the present study, we investigate chemical modifications in a Cu/WC tribo-system under high tribological loading. The major research focus is to investigate the nucleation and growth processes of Cu oxide by using high-angle annular dark-field scanning transmission electron microscopy (HAADF-STEM) through differences in atomic number (Z) contrast and atom probe tomography (APT). The prevailing mechanisms will be critically appraised by tracking chemical modifications at different stages during sliding contact.

Oxygen-free high conductivity pure Cu (Goodfellow, Shanghai, China) with a purity of 99.995% was chosen for subsequent friction tests. The hardness is about 0.7 GPa and the grain size is ~200 μm in average. Dry friction tests of the coarse-grained Cu samples were carried out with an Optimol SRVIII reciprocating tribometer in ball-on-plate contact sliding against WC balls with minor Co element, immediately after electro-polishing of the Cu samples. The WC ball is 10 mm in diameter and its roughness is 0.037 $\pm$ 0.011 μm. The normal load was 30 N and speed was kept as 10 mm/s. The stroke length was 1 mm. The maximum Hertzian contact pressure is 1.44 GPa, which was calculated with a Young's modulus of 117 GPa for Cu and 680 GPa for WC and a Poisson ratio of 0.34 for Cu and 0.24 for WC. The tests were conducted at room temperature in 45% relative humidity in air. To thoroughly investigate chemical changes within the Cu samples, the sliding cycles were increased from 50, 300, 3000, 6000, up to 18000 cycles.

Cross-sectional transmission electron microscopy (TEM) foils were extracted from the middle of the wear scar and parallel to the sliding direction in a focused ion beam/scanning electron dual beam microscope (Helios NanoLab 660 from FEI, Hillsborough, USA). A platinum layer was deposited on the sliding surface to protect against beam damage. The annular bright field (ABF) and high-angle annular dark field (HAADF) scanning transmission electron microscope (STEM) images were acquired using the FEI Titan ChemiSTEM G2 operated at an accelerating voltage of 200 kV. STEM-HAADF image simulations were performed with the Dr. Probe software package [22]. The specimen thickness of about 30 nm was used in simulations, consistent with the TEM lamella thickness prepared by focused ion beam. The probe was set to zero aberration. The acceleration voltage was set to 200 kV, and a convergence angle of 24.7 mrad was used, consistent with the experimental parameters. The inner and outer radii of the HAADF detector were set to 80 mrad and 250 mrad, respectively.

The chemical information was attained by performing energy dispersive X-ray spectroscopy (EDS) and electron energy loss spectroscopy (EELS) measurements in TEM. Additionally, the local chemical composition at the near atomic scale was investigated for the Cu samples using 3D atom probe tomography (APT). Laser-assisted field evaporation was employed within a local electrode atom probe (LEAP 4000X HR, CAMECA). The laser pulse energy and the frequency of the laser pulses were 40 pJ and 125 kHz, respectively. The base temperature in the analysis chamber was maintained at 60 K during the measurement. The APT tips were fabricated using the same FEI dual-beam focused ion beam system. A thin platinum layer was deposited to prevent the surface from ion beam damage and to ensure the APT tips are as close to the topmost layer of the sample as possible. Data reconstruction and analysis were carried out using the IVAS 3.8.4 software package.

Fig. 1 presents a typical coefficient of friction (COF) variation with the sliding cycles for the copper sample sliding against a WC ball with a load of 30 N and a speed of 10 mm/s. The COF increases immediately after sliding, reaching a steady value of 0.73 after sliding for about 6000 cycles. This result is in agreement with the notably rougher surface with the increasing sliding cycles (Supplementary Fig. S1). While for the contacting WC balls, plastic deformation and wear loss are trivial according to experimental characterization of surface morphology and subsurface layer (Supplementary Fig. S2). For the ball-on-plate experimental configura-

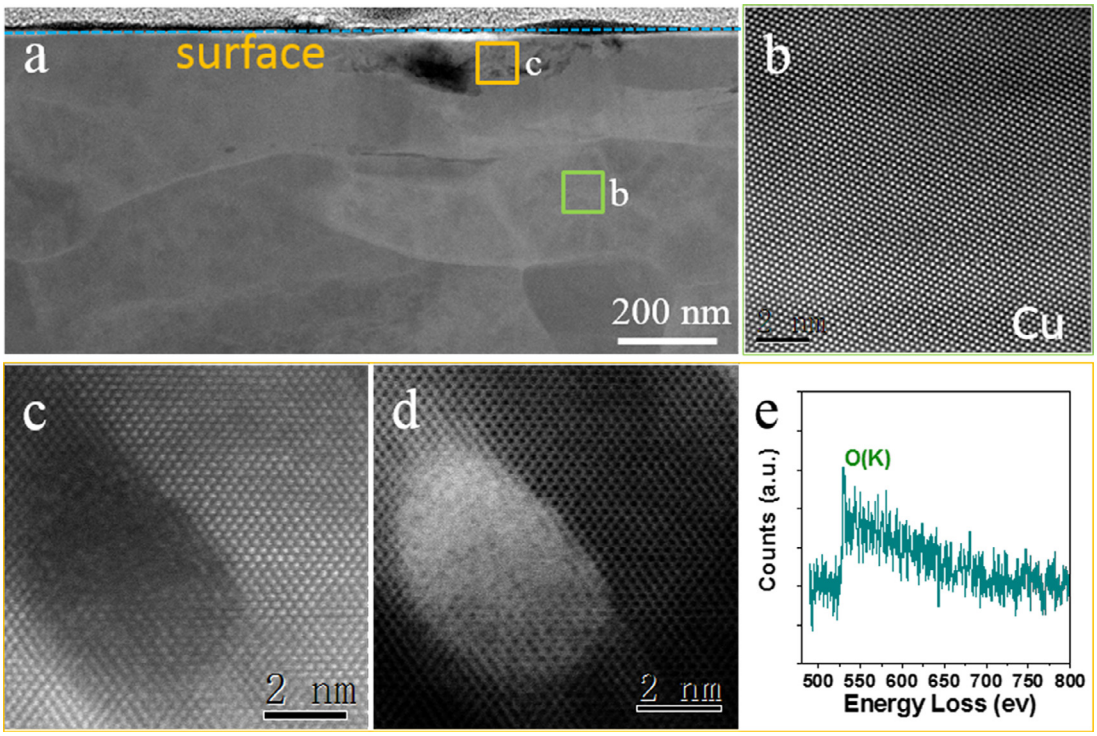

Fig. 2. (HR)STEM images for the copper sample sliding after 300 cycles: (a) an enlarged STEM image from Fig. 1c; (b) HRSTEM image taken from the light green rectangle in (a); (c–d) STEM-HAADF and ABF images from the area in the orange rectangle in (a), respectively. (e) Oxygen K-edge EEL spectra of the area indicated in (d).

tion in the present work, the Hamilton's model allows calculating the subsurface stress field [23]. In the beginning of sliding contact, the τ-component of the stress field demonstrates an applied stress level can be as high as 500 MPa for the COF of 0.45, far above the yield stress of the CG copper (about 63 MPa, [24]). While for the steady state, the calculated shear stress rises to approx. 700 MPa (Supplementary Fig. S3), suggesting the implementation of high tribological loading during all sliding cycles. Such high tribological loading can also be reflected by the microstructural refinement in the topmost layers of the samples after different sliding cycles (Fig. 1c,f). After 300 cycles, the topmost layer is made of ultra-fine grains (UFG) with an average size of 500 nm as shown in the cross-sectional STEM image (Fig. 1c). When the cycle number increases to 3000 cycles, the grain size in the topmost layer decreases to about 200 nm (Fig. 1d). This value is consistent with the saturated microstructural size reported in the literature, when dislocation manipulation and annihilation is balanced for the grain boundary migration upon large plastic deformation [25]. For the steady state of sliding (6000 and 18000 cycles), the UFG structure gradually evolves into a nanocrystalline structure, distinctly different from that under mild sliding [20]. The darker contrast in Fig. 1d,f shows evidence of transporting foreign elements into the base material during sliding, which will be further characterized.

High-resolution STEM (HRSTEM) and EELS techniques were applied to disclose the interactions between the sample and the environment occurring after 300 sliding cycles (Fig. 2). In HAADF-STEM, the image intensity is proportional to Z^2 and density, enabling Cu and its oxide to be distinguished. Some discontinuous dark regions are found in an enlarged STEM image (Fig. 2a). At a depth of about 400 nm below the surface, the HRSTEM image shows the undisturbed atomic-scale structure of Cu in a zone axis of [110] (Fig. 2b). While for the dark areas, both the HAADF and ABF images reveal that a nanoparticle of about 3 nm in size is formed inside the Cu matrix (Fig. 2c,d). The corresponding EELS measurement demonstrates that there is an energy-loss peak at about 532 eV (Fig. 2e), which corresponds well to the ionization energy of the oxygen 1s state. It is reasonable to assume the dark areas in Fig. 2a to be oxidized areas, due to a substantially reduced HAADF image intensity. Such early stage chemical change is further substantiated by APT investigations (Supplementary Figs. S4 and S5). As shown in Supplementary Fig. S4, oxygen-enriched nano particles (demonstrated by oxygen iso-concentration surface 0.5 at.%) form in the topmost layer. Similar scenario but with a lower number of nanoparticles is also captured in the sample sliding after 50 cycles (see Supplementary Fig. S5).

After 3000 sliding cycles, the dark areas are frequently seen in deeper near-surface areas in the Cu sample (Fig. 3a), compared with the sample after 300 cycles (Fig. 2). The dark area highlighted by the rectangle in Fig. 3a seemingly separates the neighboring Cu grains. The corresponding HRSTEM image resolves the Cu/Cu_2O interface at the atomic scale (Fig. 3b). Cu_2O appears to be slightly darker than Cu, consistent with their Z-contrast difference. Based on the HRSTEM image, we combine face-centered cubic (fcc) Cu and Cu_2O atom models into a supercell, both viewed along the [110] direction (Fig. 3c). The produced atom model shows the difference between two fcc phases is that oxygen atoms locate in the interstitial tetrahedral sites of Cu_2O. In addition, simulated STEM-HAADF image was obtained via Dr. Probe by matching the Cu and Cu_2O model (Fig. 3d). The Z-contrasts in Fig. 3b are in agreement with our STEM simulations. Furthermore, the fast Fourier transform (FFT) pattern of the image (Fig. 3e) demonstrates the following two facts. First, Cu and Cu_2O has a {111} // {111} crystallographic relationship. Second, the rotation between respective (111) planes is very small, basically around 1.5° according to the indexed diffraction spots. For better illustration, we compare the spacings measured along ten (111) lattice planes in Fig. 3b, which are acquired from the inverse FFT images by choosing the two spots corresponding to (111) plane in the FFT image for both structures, respectively (Fig. 3e). Line profiles (Fig. 3f) show measured lattice spacings represent the (111) spacing of Cu (2.18 Å) and Cu_2O

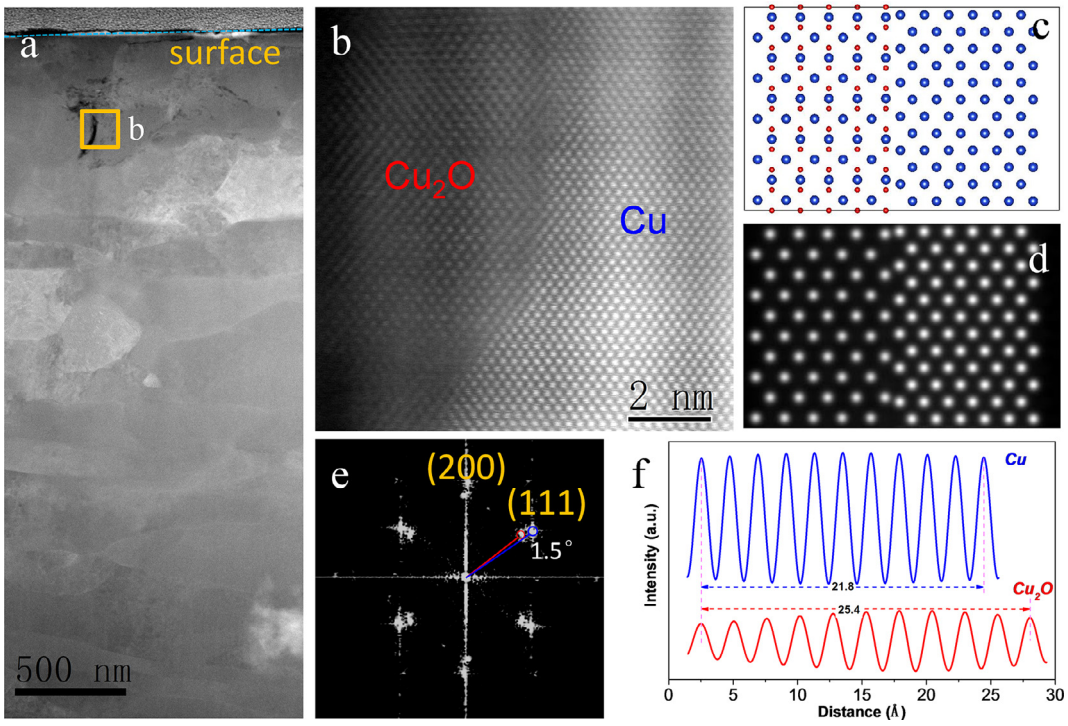

Fig. 3. (HR)STEM cross-sectional images for the copper sample sliding after 3000 cycles: (a) an enlarged STEM image from Fig. 1d; (b) HRSTEM image showing the Cu/Cu_2O interface taken from the rectangle in (a),(c) and (d) atom model for the Cu/Cu_2O interface and corresponding HRSTEM simulation, respectively. (e) FFT pattern of (b). (f) The intensity profiles perpendicular to (111) plane of inverse FFT images in (b).

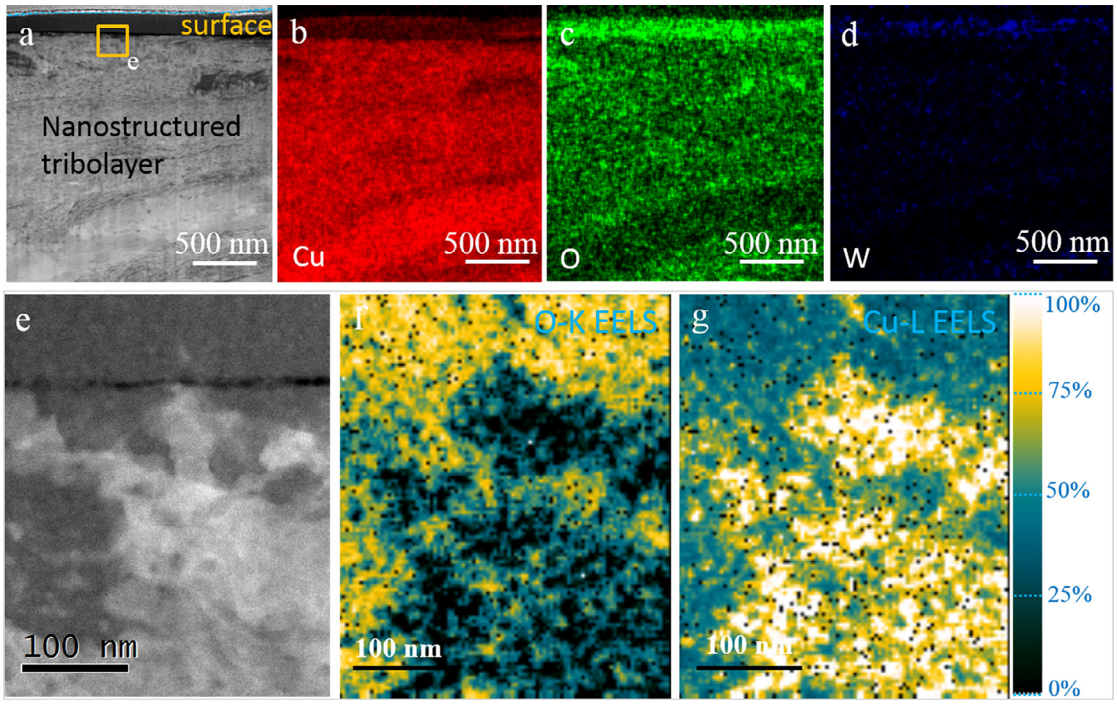

Fig. 4. STEM cross-sectional image (a) and corresponding EDS maps (b–d) for the copper sample sliding after 18000 cycles. (e) An enlarged STEM image from the rectangle indicated in (a). (f and g) Elemental chemical maps constructed by integrating the spectra: (f) O K-edge and (g) Cu L-edge. The unit is at.%.

(2.54 Å), respectively. The spacing data translates into a lattice expansion of about 17% between these two phases.

A nanostructured tribolayer is formed below the worn surface after 6000 and 18000 cycles (Fig. 4a and Supplementary Fig. S6). EDS maps show pronounced evidence of oxygen and tungsten in the tribolayer in the sample after 18000 cycles (Fig. 4b,d), while tungsten is not detected after 6000 cycles (Supplementary Fig. S4). The presence of tungsten directly verifies elemental transport from the WC ball to copper, in contrast to negligible mixing under mild sliding of Cu against a sapphire ball [20]. Note that these mixed elements are heterogeneously distributed and their contents are higher in the topmost 200 nm thick layer. A quantitative analysis

of the chemical composition by EELS mapping indicates the presence of Cu oxides and Cu solid solution in the tribolayer (Fig. 4e,g). The stoichiometric oxides cannot be easily identified, as the oxygen content is heterogeneous in distribution.

Hence, fundamental stages are identified during high tribological loading of the chosen Cu/WC tribo-system: (i) grain refinement of Cu to the UFG regime in the very beginning of sliding contact; (ii) nucleation of extremely fine oxygen-enriched particles in the subsurface layer; (iii) subsequent growth of the Cu_2O oxide in the subsurface layer; (iiii) continuous nanostructured mixing layer in the late stage.

Our present atomic scale characterization clearly demonstrates the crystallographic relationship between Cu and its oxide under high tribological loading for the first time. Note that it is not uncommon that Cu and Cu_2O have a {111} // {111} relationship, as reported in the literature [26]. While the phases present in the literature (e.g. static oxidation) were assumed to be stoichiometric oxides, it may be incorrect for the phase changes occurring under tribological loading, wherein the chemical composition in the topmost tribolayer are highly dynamic. As a result, equilibrium of phase and composition may never be reached (Fig. 4f,g). This echoes to a recent investigation that nonequilibrium solute capture occurs in the moving oxide interfaces during high temperature oxidation of NiCrMo alloys [27].

The current study suggests that near-surface mechanical mixing is presumably the main contribution to chemical modifications under high tribological loading, in addition to the proposed surface diffusion mechanism of oxygen under mild sliding [20]. This fact reveals a mechanically driven pathway for the formation of chemically modified layer. It was previously identified that dislocation-mediated plastic flow in grains is responsible for bulging and fold formation [28]. Thus, we speculate that mechanical mixing with oxygen and tungsten may be assisted by high contact stress induced shear instabilities (e.g. folds) in the near-surface layer. For the starting nucleation event, Cu and Cu_2O are crystallographically related in the stochastically near-surface areas (Fig. 3b), similar to the epitaxial growth during oxidation of thin films. Upon high loading, it is reasonable to assume that oxygen could penetrate into the interstitial tetrahedral sites while retaining the underlying fcc crystal structure. Tungsten from the counterbody was mixed into the tribolayer in the late stage. This can be understood from the fact that the elevated hardness (as high as 2 GPa) of the tribolayer enhances its mechanical mixing ability with the WC ball.

In summary, a sequence of stages are revealed by tracking chemical modifications during high tribological loading of the Cu/WC tribo-system: First, high tribological stress facilitates grain refinement to the UFG regime in the incipient stage; Second, nucleation of extremely fine oxygen–enriched Cu nano particles and subsequent growth of the Cu_2O oxide in the near-surface layer; Third, formation of nanostructured mixing layer with heterogeneous Cu and O distribution in the late stage. Near-surface mechanical mixing is supposed to contribute to elemental transport under high tribological loading. We also suspect this mechanism unavoidably occurs in many surface processing techniques such as surface mechanical contact treatments, which may be previously overlooked and should be taken into consideration.

Declaration of Competing Interest

The authors declare that they have no known competing financial interests or personal relationships that could have appeared to influence the work reported in this paper.

Acknowledgements

This work was supported by the National Natural Science Foundation of China (Grant No. 52001165 and 51931003), Natural Science Foundation of Jiangsu Province, China (Grant No. BK20200475) and the Fundamental Research Funds for the Central Universities (Grant No. 30921011215). The authors are thankful for the technical support from Jiangsu Key Laboratory of Advanced Micro&Nano Materials and Technology, and the Materials Characterization Facility of Nanjing University of Science and Technology. Dr. Baptiste Gault is sincerely acknowledged for helpful discussions on the APT results. Dr. Baptiste Gault is sincerely acknowledged for helpful discussions on the APT results.

Supplementary materials

Supplementary material associated with this article can be found, in the online version, at doi:10.1016/j.scriptamat.2021.114142.

References

[1] C. Haug, F. Ruebeling, A. Kashiwar, P. Gumbsch, C. Kübel, C. Greiner, Nat. Commun. 11 (2020) 839.
[2] W.G. Sawyer, N. Argibay, D.L. Burris, B.A. Krick, Ann. Rev. Mater.. Res. 44 (2014) 395–427.
[3] X. Chen, Z. Han, X.Y. Li, K. Lu, Sci. Adv. 2 (12) (2016) e1601942.
[4] P. Stoyanov, R. Merz, P.A. Romero, F.C. Wählisch, O.T. Abad, R. Gralla, P. Stemmer, M. Kopnarski, M. Moseler, R. Bennewitz, M. Dienwiebel, ACS Nano. 9 (2015) 1478–1491.
[5] N. Argibay, M. Chandross, S. Cheng, J.R. Michael, J. Mater. Sci. 52 (2017) 2780–2799.
[6] F. Ren, S.N. Arshad, P. Bellon, R.S. Averback, M. Pouryazdan, H. Hahn, Acta Mater. 72 (2014) 148–158.
[7] Y. Zhang, S. Descartes, R.R. Chromik, Tribol. Int. 134 (2019) 15–25.
[8] Y. Zhang, J. Michael Shockley, P. Vo, R.R. Chromik, Tribol. Lett. 62 (2016) 9.
[9] D. Rigney, S. Karthikeyan, Tribol Lett, 39 (2010) 3-7.
[10] X. Chen, R. Schneider, P. Gumbsch, C. Greiner, Acta Mater. 161 (2018) 138–149.
[11] D.A. Rigney, Wear 245 (2000) 1–9.
[12] O.J. Furlong, B.P. Miller, W.T. Tysoe, Tribol. Lett. 41 (2011) 257–261.
[13] X. Chen, Z. Han, K. Lu, Wear 320 (2014) 41–50.
[14] T.F.J. Quinn, Tribol. Inter. 16 (1983) 257–271.
[15] Q.C. Zhang, X. Chen, Z. Han, Wear 462-463 (2020) 203521.
[16] M. Kerridge, J.K. Lancaster, T.E. Allibone, in: Proceedings of the Royal Society of London. Series A. Mathematical and Physical Sciences, 236, 1956, pp. 250–264.
[17] N.N. Gosvami, J.A. Bares, F. Mangolini, A.R. Konicek, D.G. Yablon, R.W. Carpick, Science 348 (2015) 102–106.
[18] P. Stoyanov, P.A. Romero, R. Merz, M. Kopnarski, M. Stricker, P. Stemmer, M. Dienwiebel, M. Moseler, Acta Mater. 67 (2014) 395–408.
[19] N.K. Sundaram, Y. Guo, S. Chandrasekar, Phys. Rev. Lett. 109 (2012) 106001.
[20] Z. Liu, C. Patzig, S. Selle, T. Höche, P. Gumbsch, C. Greiner, Scr. Mater. 153 (2018) 114–117.
[21] J.S. Lehmann, R. Schwaiger, M. Rinke, C. Greiner, Adv. Mater. Interfaces (2020) 2001673.
[22] J. Barthel, Ultramicroscopy 193 (2018) 1–11.
[23] G.M. Hamilton, Proc. Inst. Mech. Eng. Part C-J. Eng. Mech. Eng. Sci. 197 (1983) 53–59.
[24] T.H. Fang, W.L. Li, N.R. Tao, K. Lu, Science 331 (2011) 1587–1590.
[25] X. Chen, Z. Han, X.Y. Li, K. Lu, Scr. Mater. 185 (2020) 82–87.
[26] C. Gattinoni, A. Michaelides, Surf. Sci. Repor. 70 (2015) 424–447.
[27] X. Yu, A. Gulec, Q. Sherman, K.L. Cwalina, J.R. Scully, J.H. Perepezko, P.W. Voorhees, L.D. Marks, Phys. Rev. Lett. 121 (2018) 145701.
[28] A. Gola, R. Schwaiger, P. Gumbsch, L. Pastewka, Phys. Rev.Mater. 4 (2020) 013603.